Interatomic potentials for the simulation of the zinc-blende and wurtzite forms of ZnS and CdS: Bulk structure, properties, and phase stability

Kate Wright*
Department of Chemistry and Earth Sciences, University College London, Gower Street London WC1E 6BT, United Kingdom and Royal Institution of Great Britain, Albermarle Street, London W1S 4BS United Kingdom

Julian D. Gale
Nanochemistry Research Institute, Department of Applied Chemistry, Curtin University of Technology, P.O. Box U1987, Perth 6845, Western Australia

(Received 6 January 2004; published 28 July 2004)

We present new interatomic potentials with which to model the structures and stabilities of the zinc-blende (ZB) and wurtzite (W) polytypes of ZnS and CdS. The potentials are able to reproduce many of the properties of all four minerals to within a few percent of the experimental values. In contrast to the majority of previous forcefields, the calculated relative stabilities of the cubic and hexagonal phases are found to be in the correct order for both ZnS and CdS, with the key being the inclusion of a four-body contribution to the energy. For ZnS, the cubic polytype is predicted to be the most favorable while for CdS, the hexagonal phase is the more stable. In solid solutions of $Zn_xCd_{1-x}S$ we find that the transition from hexagonal to cubic occurs for a composition of $x=0.6$.

DOI: 10.1103/PhysRevB.70.035211 PACS number(s): 91.60.−x, 62.20.−x, 64.70.−p

I. INTRODUCTION

The binary metal sulfide compounds CdS and ZnS are of long-standing interest because of their semiconducting properties, particularly since their band gaps are in a region that lends itself to technological applications. Recently there has been considerable work in the area of both materials in the context of nanostructures, with ZnS forming nanowires[1] and CdS being used to either form quantum dots, or to passivate the surfaces of other materials to create a confined particle.[2] Both sulfides can form in the hexagonal wurtzite or cubic zincblende structures, where both structure types have a tetrahedral arrangement of atoms that differ only in their stacking sequences, i.e., they are polytypes. The cubic polytype has a cubic close packing of atoms with a three-layer repeat (ABC) along the [111] axis, while the hexagonal form has hexagonal close packing with a two layer repeat (AB) along the *c* axis. The two structures can be thought of as differing in the relative handedness of the third stacking layer.

Sphalerite, the cubic form of ZnS, is considered to be more stable than wurtzite[3] although there is no firm consensus on the energy difference between the two. Standard tables of thermodynamic data[4,5] quote a difference in enthalpy of 13 kJ mol^{-1} at ambient conditions, although more recent experiments[6] give much smaller values, around 2 kJ mol^{-1}. It has even been proposed[7] that sphalerite and wurtzite are essentially the same phase, but with sphalerite being deficient in Zn relative to wurtzite. Sphalerite readily transforms to wurtzite at 1013 °C or 1031 °C depending on the activity of sulphur,[8] suggesting some link between stability and stoichiometry at higher temperatures. Many polytypes with mixed cubic/hexagonal stacking sequences are also known to occur, although the factors that control formation of these polytypes, some of which have repeat units of several hundred angstroms,[9] are still not fully understood. Pure sphalerite is rarely found in nature, but usually contains significant amounts of Fe (up to 26 wt.%) substituting for Zn, as well as Mn and Cd (up to 5%). In addition, sphalerite can contain Ga, Ge, In, Co, and Hg, which make it an important ore mineral. In contrast, cadmium sulfide is more stable as the hexagonal polytype greenockite, with the cubic phase, hawleyite, only being stable above 525 °C.[3] Unlike ZnS, complex polytypes of this phase have not been reported in the literature.

A large body of experimental information is available on the electronic structure and properties of these materials, supplemented by a growing number of theoretical results. Quantum mechanical calculations, based on density functional theory, have been used to predict a range of properties of the cubic form of ZnS (Refs. 10–13) and to examine ZnS polytypic behavior.[14,15] Recent theoretical studies of CdS in the literature, and of ZnS as well, are mainly concerned with calculations of nanoclusters.[16–18] Only a small number of studies using classical atomistic methods have been reported. These include studies of defect properties of sphalerite and wurtzite,[19] of the bulk properties of cubic CdS and ZnS,[20] as well as surface properties[21,22] and small clusters.[23] However, atomistic calculations that use interatomic potentials are now well established and can provide information on bulk and surface properties of a whole range of materials using a minimum of computational resource. Consequently, they will provide a useful means of studying the structural and energetic properties of nanostructures at the true experiment dimensions-something that is at the limit, and in many cases beyond, of what can be achieved with current *ab initio* quantum mechanical techniques.

The aim of the present study is to derive a set of consistent interatomic potential parameters that correctly predict the properties and phase stability of the cubic and hexagonal forms of CdS and ZnS. Although other potentials[19,20,22] are

able to reproduce many of the properties of sphalerite, wurtzite, greenockite, and hawleyite, they are unable to correctly predict the relative stability of the cubic and hexagonal phases. However, this is essential if we wish to make comparisons between the different structures. In particular, there is considerable interest in how the relative stabilities of the phases vary when considering nanoparticles of the materials. It has been proposed that, in some cases, the stability order is reversed from that of the bulk in the initial stages of crystal growth. As a foundation for future investigations of this important phenomena, it is necessary to derive a model that is capable of examining such behavior. In the following sections we give an overview of the methods employed and then present results for both the perfect and defective properties of ZnS and CdS.

II. METHODOLOGY

A. Theoretical background

The atomistic simulation method is based on the Born model of solids where interatomic potential functions are defined to model the long-range attractive and short-range repulsive forces acting between atoms or ions in the solid. Long-range forces are described by Coulomb's law and account for the dominant part of the energy, while the functional form of the potential used to describe short range interactions depends on the nature of the forces in the material of interest. For more ionic interactions, a two-body potential that includes an exponential repulsive term and an attractive dispersion term, such as the Buckingham potential, is commonly used:

$$U_{ij}^{\mathrm{Buck}} = A_{ij}\exp\left(-\frac{r_{ij}}{\rho_{ij}}\right) - \frac{C_{ij}}{r_{ij}^6}. \tag{1}$$

However, this term alone may not be adequate to describe the system and three- and four-body terms may also be required. For more covalent materials, the directionality can be described by inclusion of a three-body potential to represent bond-bond interactions. Here we chose to include a harmonic three-body term with exponential decay, in order that there is no discontinuous behavior with respect to atoms moving between coordination shells, which takes the form,

$$U_{jik}^{b} = \frac{1}{2}k_b(\theta_{jik} - \theta_0)^2\exp\left(-\frac{r_{ij}}{\rho_1}\right)\exp\left(-\frac{r_{ik}}{\rho_2}\right), \tag{2}$$

where k_b is the force constant, θ_0 the equilibrium three-body angle between the bonds j-i and i-k, and ρ_1 and ρ_2 control the coupling between the angle-bending and bond-stretching terms. Potential 2 has a harmonic form, which favors angles such as the 109.47° angle found in tetrahedrally coordinated environments. Given that the potential is only applied to angles where the two end atoms of the three-body potential are of the same type, the values of ρ_1 and ρ_2 are constrained to be equal. To date, only three-body interactions have been included in force field simulations of sulfides in order to account for the partial covalency of the materials. Here we explore the influence of higher order interactions through the inclusion of a four-body potential to allow for torsional effects. The form of the torsion potential used in this study includes a taper term so as to limit the spatial extent of the interaction smoothly, again to prevent discontinuous behavior as the coordination geometry varies:

$$U_{ijkl}^{t} = k_t[1 + m\cos(n\phi - \phi_0)]f(r_{ij})f(r_{jk})f(r_{kl}), \tag{3}$$

where the taper function $f(r)$ takes the form,

$$r < r_{\min}\ f(r) = 1,$$

$$r_{\min} < r < r_{\max}\ f(r) = \frac{1}{2}\left\{1 + \cos\left(\pi\frac{(r - r_{\min})}{(r_{\max} - r_{\min})}\right)\right\},$$

$$r_{\max} < r\ f(r) = 0, \tag{4}$$

where $r_{\min}$ and $r_{\max}$ are the minimum and maximum distances at which tapering is applied. In addition to the above terms, a shell-model[24] is included in order to model the effects of polarizability, particularly for anionic species.

The variable parameters in the above potential forms have been obtained by empirical fitting to crystalline properties using a least squares approach. The sum of squares, F, that determines the quality of the forcefield is defined as

$$F = \sum_{\text{observables}} w(f_{\mathrm{calc}} - f_{\mathrm{obs}})^2, \tag{5}$$

where f_{calc} and f_{obs} are the calculated and observed properties, respectively, and w is a weighting factor. During the fit, the parameter values are varied until the calculated and observed properties are as close as possible and the sum of squares (F) is at a minimum. In conventional empirical fitting, the structure is represented in the sum of squares via the forces and stresses acting on the structure. However, here we employ the alternative fitting procedure, known as relaxed fitting,[25] in which each structure is optimized prior to the calculation of the sum of squares, and the criteria used are the changes in the structural parameters. This has the advantage that it ensures that not only are the forces reduced, but also that the Hessian is well conditioned. Furthermore, the curvature related properties are correctly determined about the harmonic minimum.

In addition to perfect lattice properties, we also wish to gain insights into the nature of defects in CdS and ZnS, and to investigate solid solution behavior. In ionic and semi-ionic materials, defects are charged species and cause long-range disruption in the crystal lattice. These long-range perturbations can be effectively modelled using the approach developed by Mott and Littleton[26] where the crystal is divided into three, concentric spherical regions, R1, R2a, and R2b. In R1, which contains the defect at its center, an explicit calculation is carried out to optimize the coordinates of all ions in the region until they are at their equilibrium positions. In R2a, the ions are assumed to respond harmonically due to the forces from region 1, without explicitly considering the coupled displacements of ions within region 2a. The radius of R2b is selected so that the forces within this super sphere are purely Coulombic and the relaxation can be treated essentially as the polarization response to the net charge of the defect only. The Mott-Littleton method has the advantage

that single charged defects or small defect clusters can be considered in isolation so as to mimic infinitely dilute concentrations. In the current study, a region one size of 12 Å, containing 350 ions was found to be sufficient to converge defect energies to within 0.01 eV.

A mean-field approach has been used to include the effects of solid solution between CdS and ZnS end members, where all atoms are assigned an occupancy factor o_i that lies in the range $0 \leqslant o_i \leqslant 1$. All interactions are then scaled by the product of the relevant occupancies as

$$U_{ij}^{m-f} = o_i o_j U_{ij}. \tag{6}$$

All calculations have been performed using the program GULP.[27,28]

B. Potential derivation

The short-range potential parameters used to describe interactions in ZnS were derived by a relaxed fitting procedure, where data for the structure and elastic properties of the cubic and hexagonal phases were the observable parameters. We initially carried out the fitting procedure for the ZnS phases only, since these phases are more extensively characterized experimentally. While it is possible to perform a combined fit on both ZnS and CdS simultaneously, this will yield only a minimal change in the final results, unless undue weight is placed on the latter material, given that the deviations in the observables are similar for both phases. The Zn ion was taken to be rigid (i.e., no shell) with a fixed formal charge of 2+, while the S ion was assumed to be more polarizible and so described by a core and shell. While the total charge of the sulfide ion was constrained to be 2−, the core/shell charge split was allowed to vary. Interactions between Zn and S were described by a combination of two-body Buckingham terms and an exponentially decaying three-body potential [Eq. (4)]. After initial fitting within a two- and three-body potential model, it was found to be impossible to obtain the correct order of stability for sphalerite versus wurtzite. This can be understood since the first two coordination shells are identical for both phases. While both the two- and three-body potentials act beyond the second coordination shell, and therefore, in principle, the model could discriminate between the structures, the exponentially decaying nature prevents these outer shells from having a significant influence. In contrast, a previous force field for sulfide and selenide materials, including the present compounds, utilized the Tersoff bond order approach. Because interactions are limited to three-body contributions to the attractive bond order, this method yields identical energies for all tetrahedral polymorphs of a compound, regardless of the stacking sequence, by design.

One possible view of the reason for the energy difference of the AB vs ABC stacking sequences is because of the torsional interaction, with the cubic structure exhibiting a perfectly staggered configuration, while the hexagonal phase contains several eclipsed interactions. The degree of importance of this interaction will depend on the extent of covalency in the material. In order to allow for this, a torsional potential was included within the fitting procedure, but with a tapering function with respect to the bond distances to avoid discontinuous behavior that may cause difficulties when considering defects and surfaces where bonds are cleaved. A similar approach has been taken for torsional contributions to bond-order potentials in order to ameliorate the defects of the initial Tersoff formulation.[29]

Once the best fit set of parameters for ZnS had been obtained, given the particular choice of weights for the observables, a similar procedure was carried out for CdS, but with the S-S parameters fixed and only the Buckingham Cd-S and three-body terms allowed to vary, in order to maintain compatibility of the forcefield between materials. The torsional potential was found to make no significant contribution in the case of CdS and therefore was removed from the final refinement of the CdS parameter set.

III. RESULTS

A. Structure and elastic properties

The derived potential parameter sets for CdS and ZnS are given in Table I, with a comparison of experimental and calculated structure and properties being shown in Tables II and III. For the ZnS polytypes (Table II), we see that the structure is reproduced very well, in comparison with other theoretical studies, with the calculated cell volume being only 2.2% and 0.7% larger than the measured volume for the cubic and hexagonal phases, respectively. Yeh *et al.*[15] using the LAPW method within the local density approximation, obtained a cell volume 3.5% smaller than experiment for sphalerite and 7.8% smaller for wurtzite. Other DFT calculations of sphalerite,[10–13] using both plane wave pseudopotential, LMTO and LAPW approaches, also tend to underestimate the cell volume, which is to be expected within the local density approximation, since it is known to systematically overbind. The results of Martins *et al.*[11] Casali and Christensen,[13] and Yeh *et al.*, [15] are all highly consistent in obtaining a lattice parameter of 5.345 ± 0.01 Å, having employed LMTO or LAPW methods, while the largest deviation occurs in the planewave pseudopotential technique despite the inclusion of nonlinear core corrections.

Within force field modeling, it turns out to be extremely difficult to obtain high accuracy for the structural parameters of both the cubic and hexagonal phases with a single set of parameters. This is because the experimental structures exhibit different Zn-S bond lengths despite the strong similarity of the local coordination environment. This subtle effect is difficult to capture, even at the quantum mechanical level.

The elastic constants of sphalerite have attracted much greater attention in the literature than those of wurtzite and have been determined experimentally several times. However, there is some degree of scatter for all of the three symmetry unique values, with C_{11}, C_{12}, and C_{44} spanning the ranges 94.2–104.5, 56.8–65.3, and 34–46 GPa, respectively. At the level of the uncertainty in the experimental data C_{11} is well reproduced, though C_{12} and C_{44} are rather too soft. In the quantum mechanical studies of Agrawal *et al.*,[12] and Casali and Christensen,[13] the elastic constants were also determined within the local density approximation. As expected, the value of C_{11} is considerably overestimated in

TABLE I. Interatomic potential parameters for ZnS and CdS as derived in the present study.

Species	Charge (e)			
Zn core	+2.00			
Cd core	+2.00			
S core	+1.03061			
S shell	−3.03061			
Buckingham potential	A(eV)	ρ(Å)	C(eV/Å^6)	Cut-off (Å)
Zn core - S shell	672.288	0.39089	0.0	12.00
Cd core - S shell	1240.9518	0.371852	0.0	12.00
S shell - S shell	1200.0	0.14900	0.0	12.00
Core-shell potential	k(eV/Å^2)	Cut-off (Å)		
S core - S shell	13.302743	0.8		
Three-body potential	k(eV/rad^2)	θ_0(°)	ρ_1/ρ_2(Å)	Cut-off (Å)
S shell - Zn core - S shell	9.42834×10^6	109.47	0.3	6.0
S shell - Cd core - S shell	3.59468×10^7	109.47	0.3	6.0
Torsional potential	k_t(eV)	m/n	r_{min}(Å)	r_{max}(Å)
Zn core - S shell - Zn core - S shell	0.005	+1/+3	2.5	3.0

both cases, due to the overbinding leading to shrinkage of the lattice parameter. While the values obtained for C_{12} both accord well with each other and with the upperbound to the experimental range, the values for C_{44} span 38–60 GPa. Consequently they fail to shed light as to which end of the experimental spectrum is appropriate. Despite the uncertainties in the elastic constants, the calculated bulk modulus is within 2% of the experimental value, while the density functional estimates, which range from 82 (Ref. 11) to 105.7 (Ref. 12) are consistently too high. Considering the elastic constants for wurtzite, we find that C_{44} and C_{13} are overestimated, while the principal axis diagonal constants, C_{11} and C_{33}, are underestimated. Clearly during the fitting process a compromise has to be achieved between making sphalerite elastically too hard and causing wurtzite to be too soft. Again, despite these deviations the bulk modulus is well reproduced with an error of only 3%.

TABLE II. Calculated structures and properties of the cubic and hexagonal polytypes of ZnS, including the comparison versus experiment, where known.

	Cubic		Hexagonal	
Observable	Calc.	Expt.	Calc.	Expt.
a(Å)	5.45	5.41	3.89	3.85
c(Å)	5.45	5.41	6.20	6.29
Volume (Å^3)	161.93	158.34	81.30	80.75
U/ZnS(eV)	−33.466		−33.442	
C_{11}(GPa)	107.7	102.0	111.3	122.0
C_{12}(GPa)	59.4	64.6	55.6	58.0
C_{44}(GPa)	33.2	44.6	37.7	28.7
C_{13}(GPa)			57.9	42.0
C_{33}(GPa)			126.4	138.0
K(GPa)	75.6	77.1	76.4	74.0
ϵ_{11}^0	6.49	8.37	6.71	
ϵ_{33}^0			6.90	
ϵ_{11}^∞	4.76	5.2	4.79	
ϵ_{33}^∞			4.91	

TABLE III. Calculated structures and properties of the cubic and hexagonal polytypes of CdS, including the comparison versus experiment, where known.

	Cubic		Hexagonal	
Observable	Calc.	Expt.	Calc.	Expt.
a(Å)	5.87	5.82	4.19	4.15
c(Å)	5.87	5.82	6.66	6.73
Volume (Å^3)	202.19	196.93	101.42	100.38
U/CdS(eV)	−31.744		−31.812	
C_{11}(GPa)	89.38		102.8	86.5
C_{12}(GPa)	53.52		45.4	54.0
C_{44}(GPa)	39.11		32.4	15.0
C_{13}(GPa)			47.5	47.0
C_{33}(GPa)			113.3	96.5
K(GPa)	65.5	66.0	66.4	62.8
ϵ_{11}^0	4.65		4.56	8.70
ϵ_{33}^0				9.25
ϵ_{11}^∞	3.55		3.51	
ϵ_{33}^∞				

TABLE IV. Calculated and experimental phonon frequencies (cm^{-1}) of sphalerite (ZnS) at the Γ, X, and L points of the Brillouin zone.

Mode	Experiment	This study	Calc.[a]	Calc.[b]	Calc.[c]
TO(Γ)	277	248	238	263	289
LO(Γ)		289			
TA(X)	90	111	104	106	105
TO(X)	316	231	251	279	311
LA(X)	212	236	265	208	209
LO(X)	330	268	270	307	
TA(L)	70	94	74	83	
TO(L)	289	237	241	265	
LA(L)	195	217	239	193	
LO(L)	337	253	281	313	

[a]Reference 22.
[b]Reference 10.
[c]Reference 12.

In the case of CdS (Table III), the agreement between calculated and experimental structural parameters is also extremely good, with differences in cell volume of 1% and 2.6% for the hexagonal and cubic structures, respectively. Full elastic constants have been measured for greenockite, but for the hawleyite structure only bulk modulus information is available. In general, there is some discrepancy between calculated and measured elastic moduli in greenockite, although the bulk modulus is reproduced quite well, with an error of 6.5%. However, given that there are likely to be the errors on the measured values and the approximate nature of the model, this is an acceptable result.

B. Calculation of phonons

The phonon dispersion curves for sphalerite have been experimentally determined by Vagelatos *et al.*[30] using neutron scattering measurements. Three directions from the Γ point have been studied, namely the $[00\zeta]$, $[\zeta\zeta\zeta]$ and $[\zeta\zeta 0]$, and the phonon frequencies for the band extrema involved have also subsequently been studied using density functional methods. Since the phonon data was not included in the parameterization of the force field, this provides the first test of the new potential outside the original training set. Table IV gives the calculated phonon frequencies at the Γ, X, and L points of the Brillouin zone for ZnS in the stable sphalerite phase, along with the experimental data. Also included for comparison are the phonon data as determined by other methods, including force fields and density functional theory.

Before discussing the quantitative nature of the phonons, it is important to mention that the nonanalytic correction to the dynamical matrix, D, is employed in this study at the Γ point and other band extrema,

$$D_{i\alpha j\beta} = \frac{4\pi}{V(m_i m_j)^{1/2}} \left[\frac{(k^{\Gamma} q_i^{\mathrm{Born}})_{\alpha} (k^{\Gamma} q_j^{\mathrm{Born}})_{\beta}}{(k^{\Gamma} \epsilon^{\infty} k^{\Gamma})_{\alpha\beta}} \right], \qquad (7)$$

which is not routinely included. This correction is essential to ensure that the LO/TO splitting is obtained. In the case of the density functional results compared to, the LO mode is omitted at the zone center, since the finite difference approach used makes it difficult to correct for this, in contrast to the linear response technique. Because the value of the correction depends on the direction of measurement, k^{Γ}, due to this changing the direction in which the electric field is applied, we perform a spherical integration to average the correction at Γ. In order to evaluate the above correction, in addition to the high frequency dielectric constant tensor, we also need to know the Born effective charge tensors, q^{Born}, for the material. Here we find on-diagonal values in sphalerite of +1.29 and −1.29 for Zn and S, respectively. This demonstrates that the shell model considerably reduces the formal charges in the electrical response of the material. For comparison, the Born effective charges of wurtzite are +/−1.41 in the *ab* plane and +/−1.34 parallel to the *c* axis. Thus according to the present model the hexagonal phase appears to be the more ionic of the two. Comparing the calculated phonon frequencies for sphalerite with those measured experimentally we find that the agreement is worse than for other properties. At all the points in the Brillouin zone considered the optic modes are underestimated in the calculation by between 8% and 26%, while the acoustic modes are found to be systematically too high. Although not included in Table IV, we have calculated the phonons according to the Tersoff bond order potential model of Benkabou *et al.*[20] Because there is no electrostatic component in the model, there is no LO/TO splitting in this case. Hence all the optic modes at the Γ point occur at 386 cm^{-1}, and thus the frequencies are considerably overestimated with respect to experiment. The results of Engel and Needs,[10] from the planewave pseudopotential method, are consistently much closer to experiment, despite the large overcontraction of the unit cell. However, it should be noted that the phonons were found to be very sensitive to the pseudopotential, and the omission of nonlinear core corrections changed the frequency of one mode by a factor of 4. Consequently it is not surprising that a relatively simple forcefield model cannot achieve quantitative agreement with the phonon data, without specifically fitting it.

There have been a number of studies of the phonons of the wurtzite phase of CdS, both theoretical[31] and experimental,[32] though the most recent experimental study just presents the dispersion curves,[33] rather than numerical values at extrema of the Brillouin zone. The calculated values resulting from the present potential model are given in Table V and compared against one of the sets of experimental data. Despite the fact that there has been scatter amongst the experimental frequencies, it is clear that the three modes clustered about 233 cm^{-1} are too similar, though if the direction of approach to the Γ point is spherically averaged then the lowest frequency of this grouping falls to 225 cm^{-1}. Overall, the phonon frequencies are too low on average, even though the elastic properties are too hard with respect to experiment in the present force field.

C. Stability and defects

The internal energy of the sphalerite and wurtzite forms of ZnS and CdS calculated using our new model are presented

TABLE V. Calculated versus experimental phonon frequencies (cm^{-1}) for greenockite (CdS) at the Γ point with the LO/TO splitting calculated for approach from the direction of the A point. The vibrational modes are labeled according to the notation of Nusimovici *et al.* (Ref. 31).

Mode	Experiment[a]	Calculated
Γ_1	305	265
Γ_6	256	235
Γ_5	242	233
Γ_4	211	232
Γ_4	170	168
Γ_6	85	77

[a]Reference 32.

in Tables II and III. For zinc sulfide, we find that the cubic sphalerite phase is lower in energy by 2.32 kJ mol^{-1} relative to wurtzite while for cadmium sulfide, the wurtzite phase is more stable by 6.5 kJ mol^{-1}. In the case of ZnS, the calculated energy difference between the two phases is a function of the magnitude of the force constant k_t in the torsional potential, which favors the ABC over the AB stacking. Experimentally, the standard enthalpy difference between the two phases is usually quoted as 13 kJ mol^{-1},[4,5] although more recent studies give much smaller values. For example, Gardner and Pang[6] measure $\Delta H^0(s \rightarrow w)$ at 298.15 K $= +2.3 \pm 0.9$ kJ mol^{-1} using the modified entrainment method. In nature, the most common form of ZnS is sphalerite, and although wurtzite exists, it is generally considered to be metastable at low temperature.[3] The transition temperature has been observed [7] to occur at around 1318 K although there is some variation on this depending on the activity of S and on impurity content.[4] By contrast, we find that the hexagonal form of CdS, greenockite, is the more stable polytype by 6.5 kJ mol^{-1}. The value of ΔH for greenockite is given in the literature as -161.9 kJ mol^{-1}, however we were unable to find comparable thermodynamic data for hawleyite. Both minerals are rare and the latter usually only forms as thin coatings on sphalerite. The present results are all consistent with the stability of tetrahedral binary semiconductor structures being related to the degree of covalency, with the more covalent materials, adopting the cubic structure in order to avoid torsional repulsions. Here we find that CdS is more ionic than ZnS, and hence the observed structural preference.

The defect properties of these materials are of interest because nonstoichiometry may control their relative stability, but more importantly, will have an effect on the semiconducting properties. The Schottky defect energy (U_s) is defined as the sum of the formation energies of the individual vacancies plus the lattice energy of the phase removed at infinity as

$$U_s = V''_M + V^{\cdot\cdot}_s + U_{\text{latt}}. \tag{8}$$

Defect formation energies are given in Table VI, where Schottky energies have been calculated for the case where defects are isolated and assumed to be noninteracting, and when they are bound in a vacancy cluster. For all four mineral phases, there is a significant negative binding energy associated with the pairing of defects, suggesting that vacancy clustering will occur. The formation energy of Schottky defects in ZnS are lower in wurtzite than in sphalerite, but in CdS Schottky defect formation is slightly more favorable in the cubic phase when defects are bound. Nonstoichiometry in ZnS leading to Zn deficient wurtzite is most likely introduced via the presence of impurities such as Fe^{3+} or Mn^{3+} where Zn vacancies will form to maintain charge neutrality.

TABLE VI. Defect formation energies (eV).

Defect	Sphalerite	Wurtzite	Hawleyite	Greenockite
$V^{\cdot\cdot}_S$	20.72	20.34	20.61	20.34
$V''_{Zn/Cd}$	18.93	18.78	19.58	19.99
Schottky unbound	6.17	5.70	8.45	8.53
Schottky bound	2.81	2.58	4.40	4.45
Binding energy	−3.36	−3.11	−4.04	−4.08
M^{2+} impurity	1.87	1.68	−1.59	−1.59

Thin films[34] and nanoparticles[35] of (Zn,Cd)S solid solutions have been synthesized and studied because of their interesting properties. However, the influence of stoichiometry on phase stability in the compounds is not well known. In order to investigate this, we have carried out a series of calculations using a mean field approach to determine the composition at which the cubic-hexagonal transition occurs. The proportion of Cd on Zn sites in the cubic and hexagonal structures was increased incrementally from 0 to 100%, where the energy as a function of composition x in $Zn_xCd_{1-x}S$ is plotted for both structures in Fig. 1. We find that at $x=0.6$, the energy curves cross and thus there will be a transition from the hexagonal to the cubic structure. No experimental data for the system (Zn,Cd)S are available for comparison, however, studies of the effects of composition on the structural phase transition in (Zn,Cd)Se have been performed. The experimental work of Vlasov *et al.*,[36] using low temperature excitation emission spectra, found that poly-

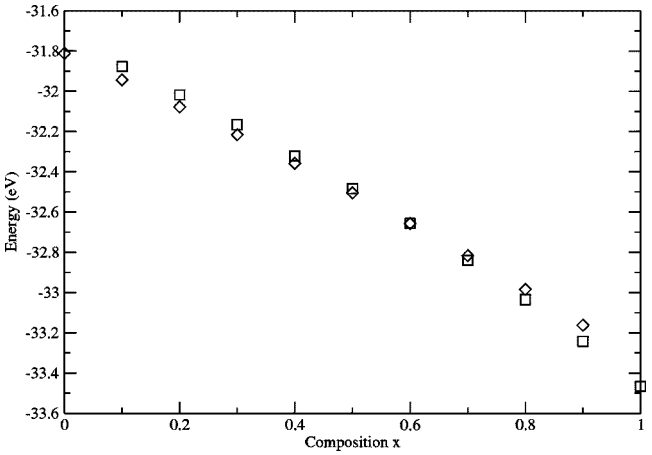

FIG. 1. Energy of the cubic (squares) and hexagonal (diamonds) polymorphs as a function of cation site composition x for the solid solution $Zn_xCd_{1-x}S$, calculated within the mean-field model.

crystals of $Zn_xCd_{1-x}Se$ have the wurtzite structure when $x<0.5$, but when $x>0.7$, they have the sphalerite structure. The transition between the two is continuous and thought to occur via the formation of stacking faults. A similar mechanism most likely operates in the sulfide system. Small amounts of Cd, or other impurities which segregate along planes, could locally change the structure from cubic to hexagonal thus leading to the formation of mixed layer polytypes. The ionic radii of Cd and Zn are 0.97 and 0.97 Å respectively, so that the larger Cd ion will exert a strain in the Zn lattice, possibly helping to drive the transition seen at 40% cadmium incorporation into ZnS in Fig. 1. This effect is also evident when considering the individual substitution energies, as given in Table VI. The smaller Zn ion can be accommodated in hexagonal CdS in larger amounts because there is less strain associated with it.

IV. CONCLUSIONS

Our new force field is able to simulate the structure and properties of the cubic and hexagonal phases of ZnS and CdS to within a few percent of the experimental values. In addition, the stability order is correctly reproduced for both compositions. A new force field that incorporates four-body interactions has been developed for the simulation of both zinc and cadmium sulfide phases. The inclusion of the torsional contribution is pivotal in being able to obtain the correct ordering of the phase stability for ZnS, where the cubic sphalerite phase is more stable than the hexagonal wurzite polymorph. In the absence of such an energetic contribution, it is impossible to stabilize the cubic phase over the hexagonal one within the standard ionic force field approach consisting of a single short-range repulsive potential, shell model and a three-body term, as demonstrated by earlier force fields. The need for a torsional potential in the case of the zinc sulfide phase is consistent with the lower Born effective charges relative to cadmium sulfide in pointing to the greater covalency of the former material as the reason for the differing structural preferences. As well as reproducing the experimental trends in phase stability, the present model also reproduces the crystallographic data and bulk moduli to within a few percent. However, as would be expected, the reproduction of the full elastic constant tensor and the dynamical matrix, as evidenced by the phonon frequencies, is less accurate. The present model predicts a phase transition for the mixed $Zn_xCd_{1-x}S$ phase to occur from the cubic to hexagonal structure when approximately 60% of the cation sites are occupied by zinc. Although this has yet to be validated experimentally, it is consistent with the equivalent trend for the selenide materials. Having determined a new force field that for the first time reliably determines the structure-energy relationships for the end member phases of these sulfide materials, it is now possible to explore the polytypism exhibited by exploring intermediate structures. Furthermore, this force field will allow the future investigation of the influence of size on the stability of sulfide nanoparticles, particularly since it is observed that at these dimensions the relative stabilities of the polymorphs can be altered through the contribution of surface effects.[37] Calculation of the properties of pure and mixed ZnS and CdS surfaces are currently underway and will form the basis of a subsequent publication.

ACKNOWLEDGMENTS

We would like to gratefully acknowledge the support of both the Royal Society, for the provision of a University Research Fellowship (K.W.), and of the Government of Western Australia for a Premier's Research Fellowship (J.D.G.).

*Electronic address: kate@ri.ac.uk

[1] X.-M. Meng, J. Liu, Y. Jiang, W. Chen, C. Lee, I. Bello, and S. Lee, Chem. Phys. Lett. **382**, 434 (2003).
[2] M. Fernee, A. Watt, J. Warner, S. Cooper, N. Heckenberg, and H. Rubinsztein-Dunlop, Nanotechnology **14**, 991 (2003).
[3] D. Vaughan and J. Craig, *Mineral Chemistry of Metal Sulfides* (Cambridge University Press, Cambridge, 1986).
[4] D. Wagman, W. Evans, V. Parker, R. Schumm, I. Harlow, S. Bailey, K. Churney, and R. Nuttall, J. Phys. Chem. Ref. Data **11**, 1 (1982).
[5] K. Mills, *Thermodynamic Data for Inorganic Sulphides, Selenides and Tellurides* (Butterworth, London, 1974).
[6] P. Gardner and P. Pang, J. Chem. Soc., Faraday Trans. 1 **84**, 1879 (1988).
[7] S. Scott and H. Barnes, Geochim. Cosmochim. Acta **36**, 1275 (1972).
[8] G. Moh, Chem. Erde. **134**, 1 (1975).
[9] S. Mardix, Phys. Rev. B **33**, 8677 (1986).
[10] G. Engel and R. Needs, Phys. Rev. B **41**, 7876 (1990).
[11] J. Martins, N. Troullier, and S.-H. Wei, Phys. Rev. B **43**, 2213 (1992).
[12] B. Agrawal, P. Yadav, and S. Agrawal, Phys. Rev. B **50**, 14881 (1994).
[13] R. Casali and N. Christensen, Solid State Commun. **108**, 793 (1998).
[14] G. Engel and R. Needs, J. Phys.: Condens. Matter **2**, 367 (1990).
[15] C.-Y. Yeh, Z. Lu, S. Froyen, and A. Zunger, Phys. Rev. B **46**, 10086 (1992).
[16] J. Joswig, S. Roy, P. Sarkar, and M. Springborg, Chem. Phys. Lett. **365**, 75 (2002).
[17] P. Deglmann, R. Ahlrichs, and K. Tsereteli, Chem. Phys. **116**, 1585 (2002).
[18] V. Gurin, Solid State Commun. **112**, 631 (1999).
[19] K. Wright and R. Jackson, J. Mater. Chem. **5**, 2037 (1995).
[20] F. Benkabou, H. Aourag, and M. Certier, Mater. Chem. Phys. **66**, 10 (2000).
[21] K. Wright, G. Watson, S. Parker, and D. Vaughan, Am. Mineral. **83**, 141 (1998).
[22] S. Hamad, S. Cristol, and C. Catlow, J. Phys. Chem. B **106**, 11002 (2002).

[23] A. Jentys, R. Grimes, J. Gale, and C. Catlow, J. Phys. Chem. **97**, 13535 (1993).
[24] B. Dick and A. Overhauser, Phys. Rev. **112**, 90 (1958).
[25] J. Gale, Philos. Mag. B **73**, 3 (1996).
[26] N. Mott and M. Littleton, Trans. Faraday Soc. **34**, 485 (1938).
[27] J. Gale, J. Chem. Soc., Faraday Trans. **93**, 629 (1997).
[28] J. Gale and A. Rohl, Mol. Simul. **29**, 291 (2003).
[29] D. Brenner, O. Shenderova, J. Harrison, S. Stuart, B. Ni, and S. Sinnott, J. Phys.: Condens. Matter **14**, 783 (2002).
[30] N. Vagelatos, D. Wehe, and S. King, J. Chem. Phys. **60**, 3613 (1974).
[31] M. Nusimovici, M. Balkanski, and J. Birman, Phys. Rev. B **1**, 595 (1970).
[32] M. Balkanski, J. Besson, and R. Le Toullec, in *Proceedings of the International Conference on the Physics of Semiconductors*, Paris, 1964 (DunodParis, 1965).
[33] A. Debernardi, N. Pyka, A. Goebel, T. Ruf, R. Lauck, S. Kramp, and M. Cardona, Solid State Commun. **103**, 297 (1997).
[34] M. Valkonen, S. Lindroos, and M. Leskela, Appl. Surf. Sci. **134**, 283 (1998).
[35] J. Cizeron and M. Pileni, Nanostruct. Mater. **8**, 419 (1997).
[36] Y. Vlasov, S. Pemogarov, A. Areshkin, and D. Fedorov, Semiconductors **30**, 241 (1996).
[37] Y. Jiang, X.-M. Meng, J. Liu, Z.-R. Hong, C. Lee, and S. Lee, Adv. Mater. (Weinheim, Ger.) **15**, 1195 (2003).